P. Z. Wang
College of Mathematics and Physics, Beijing University of Chemical Technology, Beijing 100029, China; Key Laboratory of Luminescence and Optical Information, Ministry of Education, Institute of Optoelectronic Technology, Beijing Jiaotong University, Beijing 100044, China

Prof. D. W. He, Prof. Y. S. Wang, Dr. X. X. Zhang
Key Laboratory of Luminescence and Optical Information, Ministry of Education, Institute of Optoelectronic Technology, Beijing Jiaotong University, Beijing 100044, China
yshwang@bjtu.edu.cn

Dr. J. Q. He
College of Mathematics and Physics, Beijing University of Chemical Technology, Beijing 100029, China
jqhe@mail.buct.edu.cn

Prof. Hui Zhao
Department of Physics and Astronomy, The University of Kansas, Lawrence, Kansas 66045, United States
huizhao@ku.edu

Keywords: *$PtSe_2$, Exciton, Transient absorption*

Recently, two-dimensional (2D) noble metal dichalcogenides, such as $PtSe_2$ and PdS_2, have drawn considerable attention due to their novel electronic and optical properties that can be widely tuned by thickness. However, the dynamical properties of photocarriers in these materials have been less studied. Here, photocarrier dynamics in monolayer and bilayer $PtSe_2$ samples prepared by chemical vapor deposition are studied by transient absorption microscopy. Spatially and temporally resolved differential reflectance measurements yield room temperature exciton lifetimes of 25 and 50 ps for monolayer and bilayer samples, respectively. The exciton diffusion coefficient in monolayer $PtSe_2$ is found to be as large as 48 $cm^2\ s^{-1}$. This value is higher than exciton diffusion coefficients of most known monolayer semiconductors. The deduced exciton mobility is close to the theoretical limit of charge carrier mobility of monolayer $PtSe_2$. The superior exciton transport property is unique to monolayers, as the exciton diffusion coefficient drops to 6.7 $cm^2\ s^{-1}$ in bilayers $PtSe_2$. The novel exciton transport properties, along with its high air stability, make monolayer $PtSe_2$ an attractive material for ultrathin excitonic devices. These results provide insights on the exciton dynamic properties of 2D $PtSe_2$ and help develop fundamental understanding on the performance of various optoelectronic devices based on 2D $PtSe_2$.

1 Introduction

The recent success on developing two-dimensional (2D) materials based on transition metal dichalcogenides (TMD) [1] have stimulated broader exploration of other 2D systems. Among them, noble metal dichalcogenides with the general formula of NX_2 (where N = Pt, Pd and X = S, Se, Te) have drawn considerable attention due to their interesting thickness-tunable electronic and optical properties. [2, 3, 4] For example, while bulk $PtSe_2$ has been well known for a long time as a zero-gap semimetal, [5] its 2D form was widely studied only recently. [6] Monolayer and few-layer $PtSe_2$ can now be fabricated by an array of techniques, including Pt film selenization, [7, 8, 9] chemical vapor deposition (CVD), [10, 11, 12, 13] molecular beam epitaxy, [14] and exfoliation of bulk crystals. [15, 16, 17, 18, 19] $PtSe_2$ nanofilms usually form a 1*T* lattice, [7, 20, 9] although its hexagonal phase has also been reported. [20, 10, 11] Angle-resolved photoemission spectroscopy, optical spectroscopy, and density functional theory (DFT) established that monolayer $PtSe_2$ is an indirect semiconductor with a band gap of about 1.2 eV. [7, 21, 15, 22] Increasing the thickness, the band gap shrinks quickly [14, 23, 24] with a semiconductor-to-metal transition occurring in the few-layer range. [16] Transport measurements revealed that room-temperature charge carrier mobilities of semiconducting 2D $PtSe_2$ can be as high as 210 $cm^2\ V^{-1}\ s^{-1}$, [15, 25] although typically measured values are on the order of 1 - 10 $cm^2\ V^{-1}\ s^{-1}$. [10, 16, 26, 27, 18, 28, 29, 30] Moreover, both p and n types of doping were achieved, [28] illustrating the feasibility of forming p-n homojunctions. Furthermore, 2D $PtSe_2$ also possesses interesting spin properties [8] such as defect-induced magnetism, which allows atom-by-atom engineering of its magnetic properties. [31, 32, 33]

This is the author manuscript accepted for publication and has undergone full peer review but has not been through the copyediting, typesetting, pagination and proofreading process, which may lead to differences between this version and the Version of Record. Please cite this article as doi: 10.1002/lpor.202100594

The novel properties revealed by these studies make 2D $PtSe_2$ an attractive material for many applications. In particular, recent investigations have demonstrated integration of 2D $PtSe_2$ in various devices with high performance, such as field-effect transistors, [15, 29] photovoltaic devices, [11] photodetectors [11, 15, 27, 34, 35, 36] with mid-infrared spectral range [17, 18, 37] and high speed, [38, 39] ultrathin meta-optical devices, [40] gas [11] and pressure sensors, [41] and catalysis devices. [7, 13, 42] In these applications, the dynamical properties of photocarriers often play a key role in determining the device performance. However, studies on photocarrier dynamics in 2D $PtSe_2$ are relatively rare. In particular, the predicted high charge carrier mobility [43] in monolayer $PtSe_2$ has yet to be experimentally achieved.

Here we report an experimental study on the photocarrier dynamics in monolayer and bilayer $PtSe_2$ samples fabricated by CVD. Transient absorption spectroscopic measurements establish a direct transition at about 1.85 eV in monolayer $PtSe_2$. By spatially and temporally resolving the differential reflectance associated with this transition, an exciton lifetime of 25 ps and an exciton diffusion coefficient of 48 cm^2 s^{-1} are obtained. The large diffusion coefficient corresponds to an exciton mobility of 1800 cm^2 V^{-1} s^{-1}. For comparison, the lifetime and diffusion coefficient of excitons in bilayer $PtSe_2$ are 50 ps and 6.7 cm^2 s^{-1}, respectively. These results provide insights on the photocarrier dynamics in 2D $PtSe_2$ that are useful for developing fundamental understanding on the performance of various optoelectronic devices based on 2D $PtSe_2$. In particular, the novel exciton transport properties make monolayer $PtSe_2$ an attractive material for ultrathin excitonic devices.

2 Results and Discussion

2.1 $PtSe_2$ monolayer and bilayer samples

The $PtSe_2$ monolayer and bilayer samples used in this study are acquired from 6 Carbon Technology Corporation, which are fabricated on c-cut sapphire substrates by CVD. Figure 1(a) illustrates schemat-

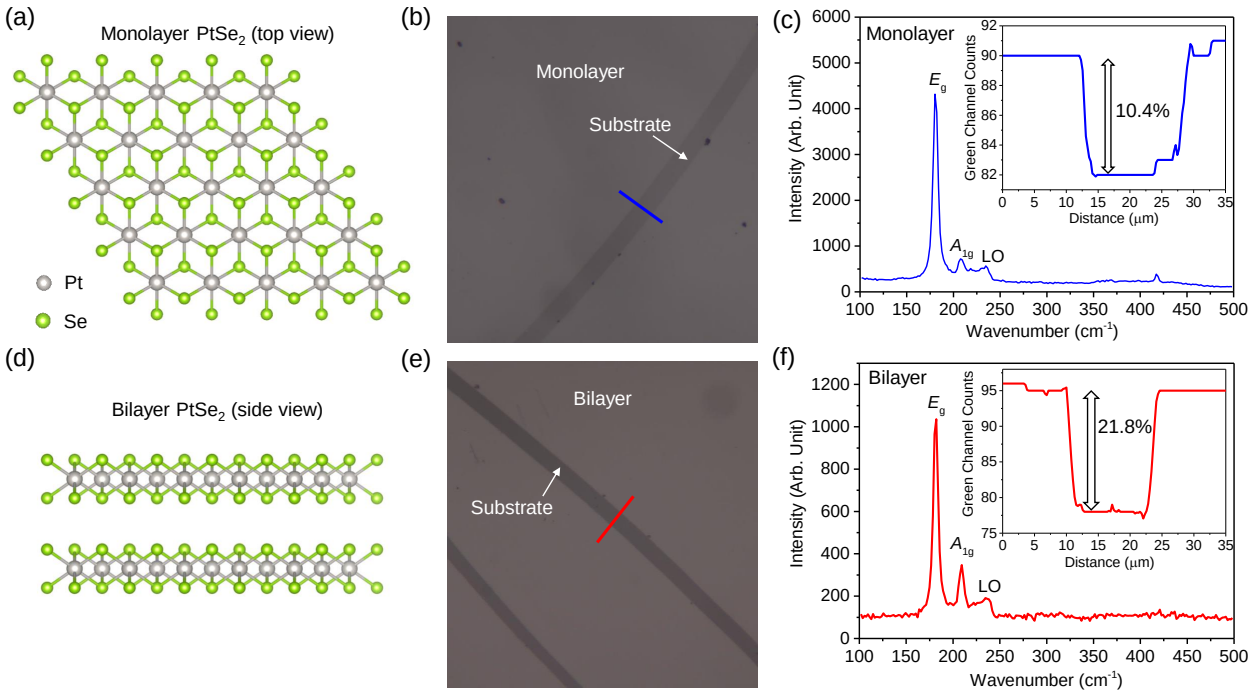

Figure 1: (a) Schematics of the crystalline structure of monolayer $PtSe_2$ (top view). (b) Optical microscope image of a monolayer $PtSe_2$ sample. (c) Raman spectrum of the monolayer $PtSe_2$ sample measured with a 532-nm laser. The inset shows the green channel profile across the blue line shown in (b). (d), (e), and (f) show the corresponding results of bilayer $PtSe_2$.

ically the atomic structure of monolayer $PtSe_2$, with a $1T$ lattice structure, where a Pt layer is sandwiched by two layers of Se atoms. An optical microscope image of the monolayer sample is shown in Figure 1(b). A region of the sample is intentionally scratched by a sharp pen to expose the substrate (the dark strip). The green channel counts across the blue line in (b) is shown in the inset of (c). The relative contrast of 10.4 % is in line with a typical monolayer semiconductor on a thick and transparent substrate, [44, 45] confirming the monolayer thickness of the sample. Figure 1(c) shows the Raman spectrum of the sample measured with a 532-nm laser. The two main peaks at 181 cm^{-1} and 209 cm^{-1} are assigned to the in-plane (E_g) and out-of-plane (A_{1g}) lattice vibration modes, respectively, according to previous reports. [11, 14, 19, 15, 34] The intensity ratio of the A_{1g} and E_g peaks of about 0.07 confirms the monolayer thickness, according to the previously established thickness-dependence of this ratio. [19] The small feature at about 230 cm^{-1} is identified as the longitudinal optical (LO) mode. [9] The crystalline structure and the characteristics of the bilayer $PtSe_2$ sample are shown in Figure 1(d) - 1(f) in a similar fashion. The reflection contrast shown in the inset of (f) is about twice of the monolayer value, as expected. Furthermore, the intensity ratio of the A_{1g} and E_g modes is about 0.26, which is consistent with its bilayer thickness. [19]

2.2 Photocarrier dynamics in monolayer $PtSe_2$

Figure 2(a) illustrates the electronic band structure of monolayer $PtSe_2$ according to a DFT calculation, [23] which shows an indirect band gap of about 1.3 eV (Γ-X) and a direct band gap of about 1.6 eV at the Γ point. Other theoretical works have predicted similar band structures, although with different values of the band gaps. [7, 21, 14, 23, 24] To identify the direct band gap, transient absorption spectroscopic measurements are performed. A 3.02-eV pump pulse excites electron-hole pairs in the high-energy states of the sample, as shown by the blue arrow in Figure 2(a). Differential reflectance of a probe pulse is measured to study the dynamics of these photocarriers. Here, the differential reflectance is defined as

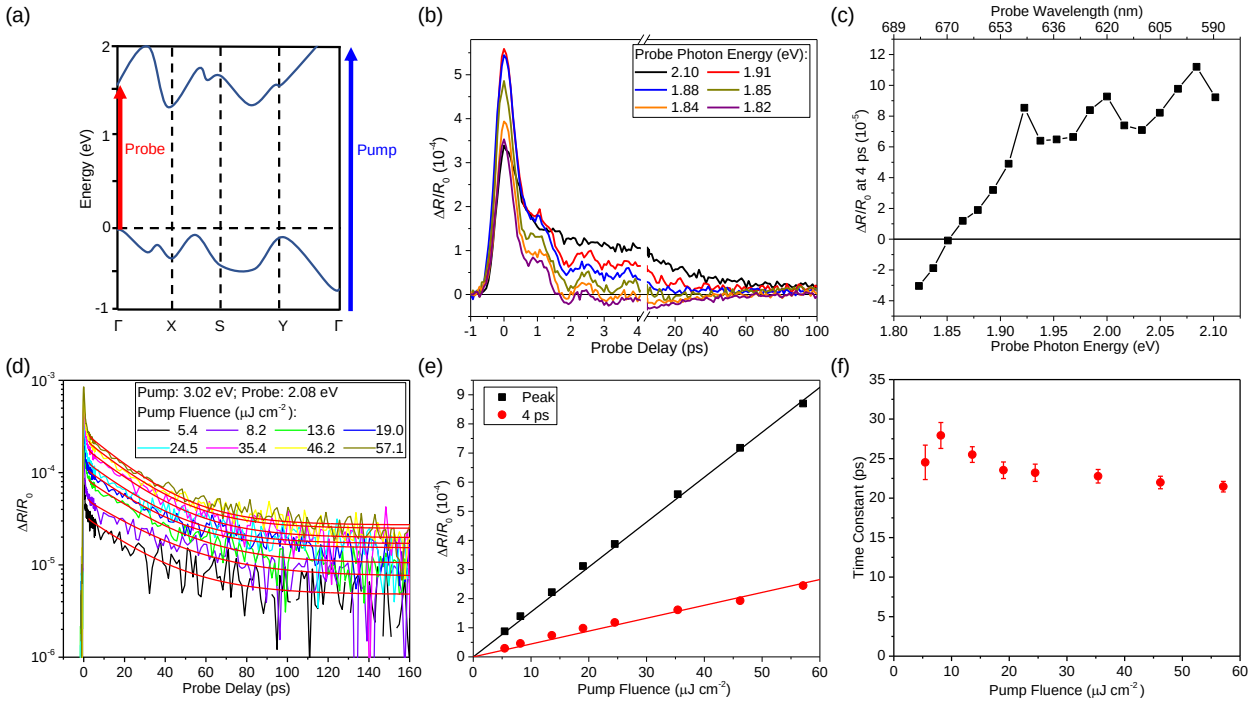

Figure 2: (a) Schematics of the monolayer $PtSe_2$ band structure and the pump-probe configuration. (b) Differential reflectance measured with a 3.02-eV pump pulse and a probe pulse of various photon energies as labeled. (c) Differential reflectance at 4 ps as a function of the probe photon energy. (d) Differential reflectance measured with a 3.02-eV pump and a 2.08-eV probe pulses, with various pump fluences as labeled. The red curves are exponential fits. (e) Peak differential reflectance and that of 4 ps as a function of the pump fluence. The lines are linear fits. (f) Decay time constant as a function of the pump fluence.

$\Delta R/R_0 = (R - R_0)/R_0$, where R and R_0 are the probe reflectance by the sample with and without the pump pulse, respectively. Figure 2(b) shows a few examples of the time-dependent differential reflectance signal with several probe photon energies. With each probe photon energy, an oscillatory feature is observed at early probe delays, which is followed by a slower decay of up to 100 ps. To describe the photon energy dependence of the signal magnitude without the complications due to the oscillatory feature, the signal at 4 ps (that is, after the oscillatory feature disappears) is plotted as a function of the probe photon energy in Figure 2(c). For photon energies above 1.85 eV, the signal is positive, showing that the absorption coefficient of the sample is reduced by the pump. Such a photobleaching effect is consistent with the absorption saturation of interband transitions due to photocarriers. [46] Below 1.85 eV, the negative differential reflectance indicates photoinduced absorption, which originates from Drude-like intraband absorption of the carriers. [47] Hence, these results suggest the existence of a direct optical band gap at about 1.85 eV.

Next, the identified direct transition is used to study the photocarrier dynamics. Figure 2(d) shows the differential reflectance signal measured with a 2.08-eV probe pulse as a function of the probe delay, with different 3.02-eV pump fluences as labeled. To estimate the pump-injected carrier density from the fluence, we adopt an absorption coefficient of 2×10^7 m^{-1} at the pump photon energy from a spectroscopic ellipsometry measurement. [22] By using Beer's law and assuming that every pump photon absorbed excites one electron-hole pair, a pump pulse of 1 μJ cm^{-2} is estimated to inject a peak carrier density of about 5×10^{10} cm^{-2}. As shown in Figure 2(e), both the peak signal and the signal at 4 ps are proportional to the pump fluence. Hence, the differential reflectance is proportional to the carrier density. By fitting the decay of the signal after the oscillatory feature with an exponential expression, $A\exp(-t/\tau) + B$, shown as the red curves in Figure 2(d), the decay time constants are deduced, as shown in Figure 2(f) as a function of the pump fluence. We attribute the exponential decay of the signal to the recombination of the photocarriers. The constant B represents a slow-varying (treated as time-independent) component of the signal, which only accounts for a few percent of the total signal. Such a background is often observed in transient absorption measurements of 2D materials [46] and could be due to lattice heating or defect-trapped carriers. Its existence does not impact the analysis of the photocarrier lifetime based on the exponentially decaying component of the signal.

Previously, photocarrier and lattice dynamics in 2D $PtSe_2$ have been studied by several groups. [6] Coherent lattice vibrations in few-layer $PtSe_2$ were recently observed. [48, 49] Thickness-dependent carrier dynamics on picosecond time scales were studied by differential transmission measurements, [50, 51, 52, 53, 54] while ultrafast Auger carrier dynamics in few-layer $PtSe_2$ samples were revealed by visible-pump-THz-probe measurements. [55] The oscillating feature observed in our experiment is due to coherent lattice vibrations, with the period and decay time being both consistent with previous results. [48, 49] The monotonic decay of the signal after the oscillating feature can be attributed to the recombination of the pump-injected photocarriers. Since a recent theory has predicted an exciton binding energy of 0.6 eV in monolayer $PtSe_2$ due to the reduced dielectric screening, [56] which is much larger than the room temperature thermal energy of 26 meV, it appears safe to assume that the photocarriers are mainly in the form of excitons. The deduced exciton lifetime of about $\tau = 25$ ps in monolayer $PtSe_2$ is on the same order of magnitude with the previously studied semiconducting TMDs, such as MoS_2 and WS_2, and can be attributed to nonradiative recombination of the excitons. [46] It is interesting to note that even at the highest injection density used in this study of about 3×10^{12} cm^{-2}, the exciton recombination dynamics remain independent of the exciton density. No signs of exciton-exciton annihilation, such as faster and nonexponential decay of the differential reflectance signal at higher densities, [57, 58] were observed.

Transient absorption microscopy measurements are performed to study the in-plane diffusion of the excitons in monolayer $PtSe_2$. As a powerful tool with high spatial and temporal resolution, transient absorption microscopy has been widely used to study ultrafast photoexcitation dynamics in various systems such as semiconductor quantum wells, [59] organic semiconductors, [60] 2D materials, [61, 62, 63] and organic-inorganic perovskites. [64, 65, 66] Details about this technique and its applications have been

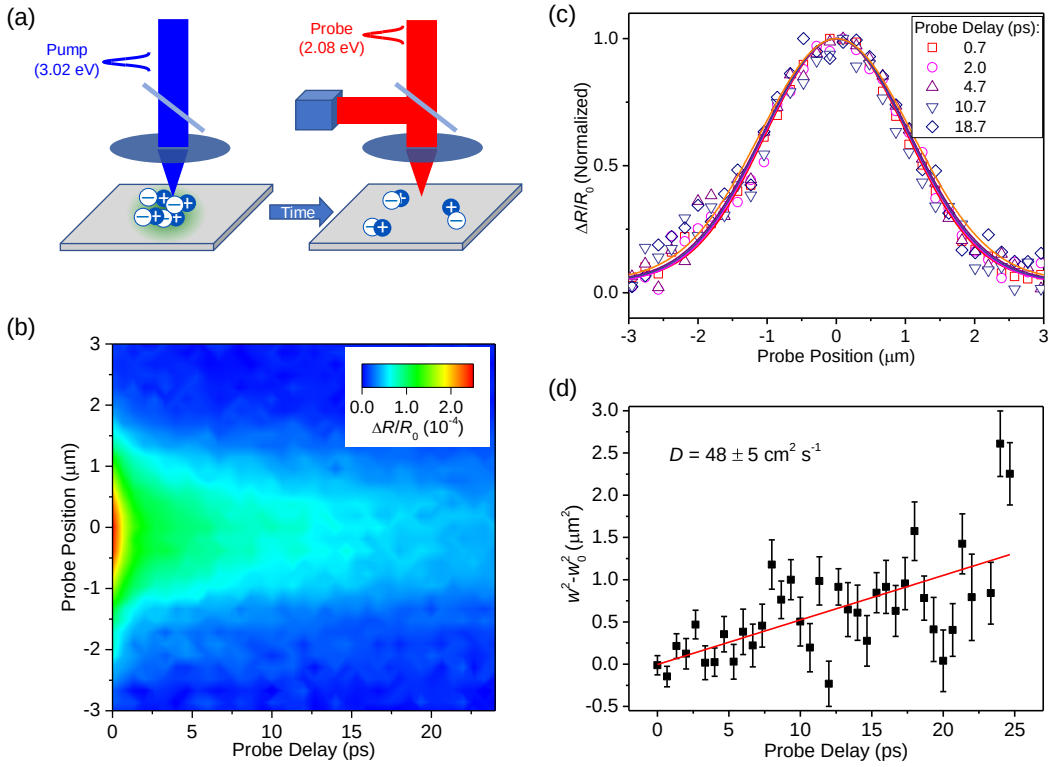

Figure 3: (a) Spatially resolved differential reflectance measurement of exciton diffusion in monolayer $PtSe_2$. (b) Differential reflectance as a function of the probe delay and probe position. (c) Examples of the spatial profiles of the signal at various probe delays (normalized). The curves are Gaussian fits to the data. (d) Squared width broadening of the profile as a function of the probe delay. The red line is a linear fit to the data that gives a diffusion coefficient of 48 cm^2 s^{-1}.

discussed in recent reviews. [67, 68, 69] In our measurements, as schematically illustrated in Figure 3(a), the tightly focused 3.02-eV pump pulse injects electron-hole pairs, which form excitons with a Gaussian spatial profile with a full width at half maximum (w) of about 1.7 μm. Driven by their density gradient, the excitons diffuse in the sample, resulting in a broadening of the profile over time. This process is monitored by the tightly focused 2.08-eV probe pulse. Figure 3(b) shows the spatiotemporal evolution of the differential reflectance signal measured by scanning both the probe delay and the probe spot position. It reflects the spatiotemporal dynamics of the exciton density, $N(r,t)$, which is described by the classical diffusion-recombination equation, [70]

$$\frac{\partial N(r,t)}{\partial t} = D\nabla^2 N(r,t) - \frac{N(r,t)}{\tau}, \tag{1}$$

where D is the exciton diffusion coefficient. With an initial Gaussian distribution with a width w_0, the exciton density profile remains Gaussian as

$$N(r,t) = \frac{w_0^2}{w^2(t)} N_0 \exp(-t/\tau)\exp[-4\ln(2)r^2/w^2(t)], \tag{2}$$

with the width broadens as

$$w^2(t) - w_0^2 = 16\ln(2)Dt. \tag{3}$$

A few examples of the normalized signal profiles are shown in Figure 3(c). By Gaussian fits (curves), the squared widths are deduced, as plotted in Figure 3(d) as a function of the probe delay. By a linear fit, an exciton in-plane diffusion coefficient of 48 $\pm$ 5 cm^2 s^{-1} is deduced. Along with the exciton lifetime of 25 ps, an exciton diffusion length of $\sqrt{D\tau}$ = 350 nm is obtained. We note that the overall exponential decay of the signal, as shown in Figure 2(d), does not impact the measurement of the diffusion coefficient, since it causes decrease of the overall profile without altering its width, as can be directly seen in Eq. 2.

The large exciton diffusion coefficient observed here further solidifies monolayer $PtSe_2$ as a novel 2D semiconductor for high-performance optoelectronic devices, especially those utilizing excitons as the energy or information carrier. For comparison, the room-temperature exciton diffusion coefficients of the mostly studied 2D semiconductors, such as TMDs, are on the order of 1 - 10 cm^2 s^{-1}. [71, 72, 73] It is also interesting to compare the exciton transport property measured here with the previously reported charge transport properties of 2D $PtSe_2$. Theoretically, 2D $PtSe_2$ was predicted to have room temperature charge carrier mobilities as high as 2000 cm^2 V^{-1} s^{-1}. [43] Recently, several groups have measured the room-temperature charge carrier mobilities in $PtSe_2$ field effect transistors. Typical values reported are in the range of 1 - 10 cm^2 V^{-1} s^{-1}, [16, 26, 27, 18, 28, 30] while higher values up to 210 cm^2 V^{-1} s^{-1} have also been achieved. [15, 25, 29] The large variation of the results could reflect the development of the sample fabrication techniques. From the measured exciton diffusion coefficient of 48 cm^2 s^{-1}, an exciton mobility of about 1800 cm^2 V^{-1} s^{-1} is deduced by using the Einstein relation, $\mu = De/k_BT$, where e, k_B, and T are the elementary charge, the Boltzmann constant, and the temperature, respectively. This value is comparable to the theoretical limits on the charge carrier mobility of monolayer $PtSe_2$. [43] Since excitons are neutral quasiparticles, their scattering with phonons and lattice defects is expected to be weaker than the charge carriers. Hence, it is reasonable that the excitons have a higher mobility than the charge carriers. Furthermore, the all-optical technique used here does not involve device fabrication and thus probes the intrinsic properties of the material.

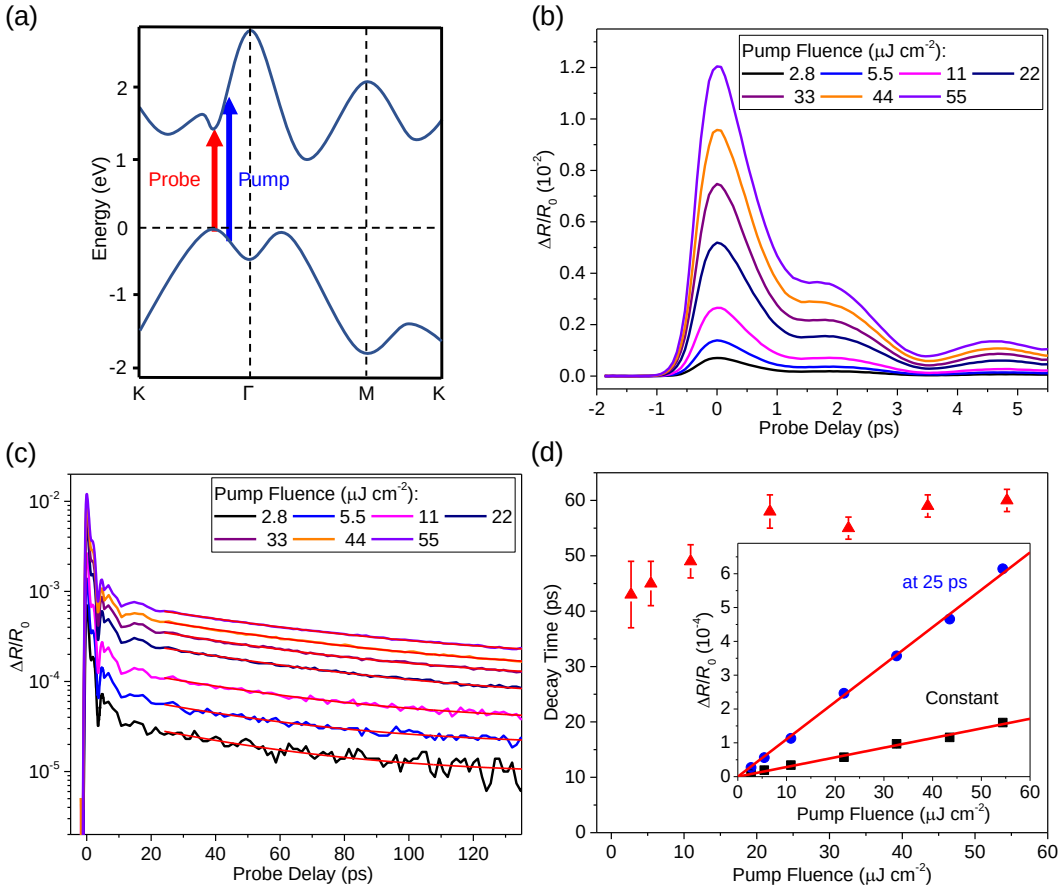

Figure 4: (a) Schematics of the bilayer $PtSe_2$ band structure and the pump-probe configuration, where photocarriers are injected by a 2.01-eV pump pulse and are detected by a 1.51-eV probe pulse. (b) Differential reflectance over a short time range measured with different pump fluences as labeled. (c) Same as (b) but over a long time range. The red curves are exponential fits. (d) Decay time constants deduced from the exponential fits shown in (c). The inset shows the signal at 25 ps and the constant term in the fit as a function of the pump fluence.

2.3 Photocarrier dynamics in bilayer $PtSe_2$

To investigate if the remarkably large exciton diffusion coefficient is unique to monolayers, the experiments are repeated on the bilayer $PtSe_2$ sample shown in Figure 1(e). The band structure of bilayer $PtSe_2$ is plotted in Figure 4(a), which shows an indirect band gap of about 1.0 eV and a direct band gap of about 1.5 eV involving states between Γ and **K** points. [23] In the measurements, a 2.01-eV pump pulse (blue arrow) excites electrons and holes in high energy states in the conduction and valence bands, respectively. A 1.51-eV probe (red arrow) senses the excited photocarriers by coupling to the direct transition.

Figure 4(b) and 4(c) show the measured differential reflectance signal on short and long time scales, respectively, with various pump fluences as labeled. For bilayer $PtSe_2$, a 1 μJ cm^{-2} pump pulse injects a peak carrier density of about 10^{11} cm^{-2}. As shown in Figure 4(b), the short-range signal is dominated by the oscillatory feature, which is similar to the monolayer sample. The rest of the signal decays exponentially and can be well fit by $A\exp(-t/\tau) + B$, as shown by the red curves in Figure 4(c). Both the signal at 25 ps and the constant B are proportional to the pump fluence, as shown in the inset of Figure 4(d), confirming that the time evolution of the signal reflects that of the photocarrier density. The decay time is found to be on the order of 50 ps. Similar to the discussions on the monolayer results, the photocarriers are expected to form excitons, and the decay time constant is attributed to the exciton lifetime, which is a factor of two longer than that of monolayer $PtSe_2$.

Finally, the in-plane diffusion of the excitons in bilayer $PtSe_2$ is studied by transient absorption microscopy measurements. Figure 5(a) shows the spatiotemporal evolution of the signal with a peak carrier density of about 5×10^{12} cm^{-2}. A few examples of the normalized signal profiles are shown in Figure 5(b). By Gaussian fits (curves), the evolution of the squared width is obtained, as shown in Figure 5(c). The linear fit shown as the red line gives an exciton diffusion coefficient of 6.7 ± 1.7 cm^2 s^{-1}. This quantity

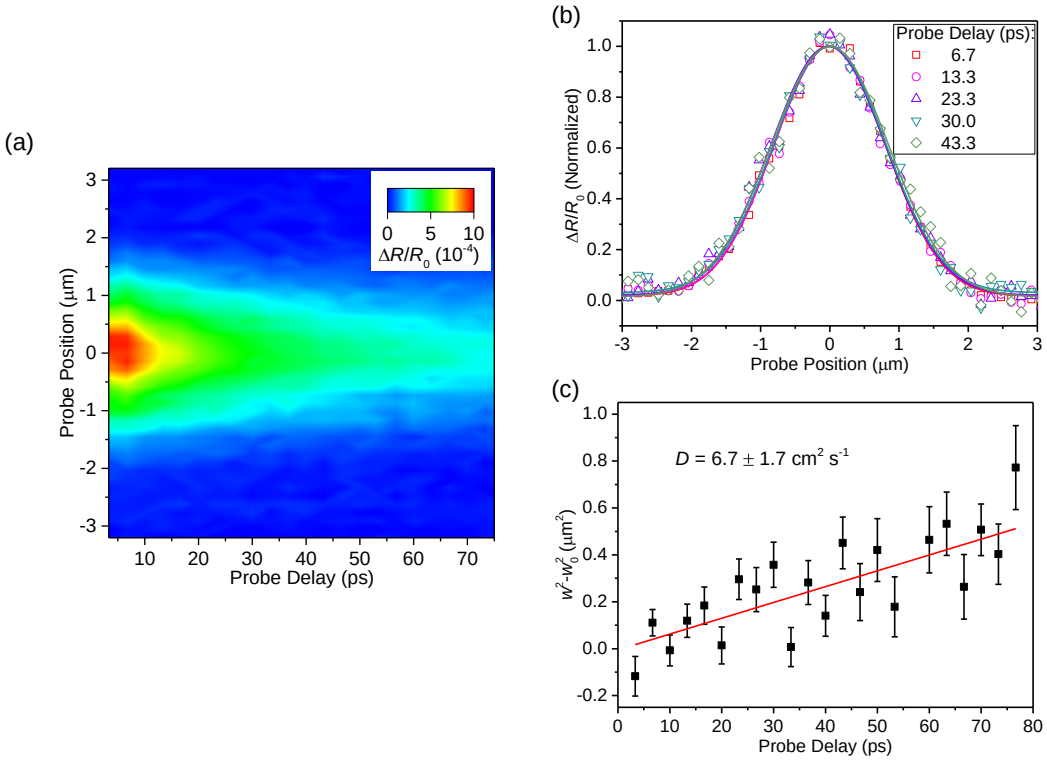

Figure 5: (a) Differential reflectance as a function of the probe delay and probe position measured from the bilayer $PtSe_2$ sample. (b) Examples of the normalized spatial profiles of the signal at various probe delays. The curves are Gaussian fits to the data. (c) Squared width broadening of the profiles as a function of the probe delay. The red line is a linear fit to the data that gives a diffusion coefficient of 6.7 cm^2 s^{-1}.

is about 7 times smaller than the monolayer exciton diffusion coefficient. Furthermore, by using the simultaneously measured exciton lifetime of about 50 ps, we obtain an exciton diffusion length of 180 nm for bilayer $PtSe_2$. The diffusion measurements of both monolayer and bilayer $PtSe_2$ are reproducible, as shown in Figure S1 and S2. We note that in order to measure the lower diffusion coefficient compared to the monolayer samples, here, a smaller laser spot (1.3 μm) is used. However, as shown in Eq. 3, the laser spot size, and thus the initial width of the exciton profile, does not affect deduction of the exciton diffusion coefficient.

3 Conclusions

In summary, photocarrier dynamics in CVD monolayer and bilayer $PtSe_2$ samples is studied by transient absorption microscopy. Both coherent lattice vibrations and carrier-induced transient absorption are observed. Spatiotemporal resolution of the carrier-induced differential reflectance signal in monolayer $PtSe_2$ at room temperature revealed an exciton lifetime of 25 ps, a diffusion coefficient of 48 $cm^2\ s^{-1}$, a diffusion length of 350 nm, and an exciton mobility as large as 1800 $cm^2\ V^{-1}\ s^{-1}$, approaching the theoretical limit of charge carrier mobilities of this material. These quantities are also measured in bilayer $PtSe_2$ for comparison. The results provide insights on the photocarrier dynamical properties of 2D $PtSe_2$. In particular, the fast exciton diffusion observed here indicates a rather high exciton mobility in monolayer $PtSe_2$, further highlighting its potential as a novel monolayer semiconductor for electronic and optoelectronic applications.

4 Experimental Section

The photocarrier dynamics are studied by transient absorption microscopy in the reflection geometry as schematically shown in Supporting Information (Figure S3). An 80-MHz mode-locked Ti:sapphire laser generates 100 fs pulses with a central wavelength of 820 nm. A portion of this pulse is used to pump an optical parametric oscillator (OPO) to produce a signal output with a central wavelength in the range of 490-750 nm. The rest of the 820-nm pulse is used directly for the measurement or sent to a nonlinear optical crystal to generate its second harmonic at 410 nm. Two of these pulses are used as pump and probe in a certain experimental configuration, which are combined by a beamsplitter and focused on the sample through a microscope objective lens. The reflected probe is sent to a photodetector through a series of filters, which block the unwanted pump reflection. The voltage output of the photodetector is measured by a lock-in amplifier. The intensity of the pump pulse is modulated by a mechanical chopper at 2.69 KHz, which is synchronized with the lock-in amplifier. With this configuration, the lock-in amplifier measures the differential reflectance ($\Delta R/R_0$), which reflects the change of the complex index of refraction of the sample at the probe wavelength induced by the photocarriers injected by the pump. Hence, the spatiotemporal evolution of this signal after the pump excitation monitors the dynamics of the pump-injected photocarriers. The differential reflectance signal is measured as a function of the probe delay, which is controlled by using a retroreflector on a motorized linear stage. To probe spatial distribution of the photocarriers, the differential reflectance is also measured as the probe spot is scanned across the pump spot by altering the incident angle of the probe into the objective lens, by tilting the beamsplitter that reflects the probe. All measurements are performed with the sample under ambient condition and at room temperature.

Supporting Information

Supporting Information is available from the Wiley Online Library or from the author.

Acknowledgements

Y.W. and D.H. are grateful to acknowledge the finical support from National Natural Science Foundation of China (Grant No.: 61875236, 61905010, 61975007) and Beijing Natural Science Foundation of China (Grant No.: Z190006). J.H. acknowledges the Fundamental Research Funds for the Central Universities (buctrc202003). X.Z. acknowledges the financial support from National Nature Science Foun-

dation of China (Grant No.: 11974088). H.Z. is supported by the U.S. Department of Energy, Office of Basic Energy Sciences, Division of Materials Sciences and Engineering under Award DE-SC0020995.

References

[1] Q. H. Wang, K. Kalantar-Zadeh, A. Kis, J. N. Coleman, M. S. Strano, *Nat. Nanotechnol.* **2012**, *7* 699.

[2] A. D. Oyedele, S. Z. Yang, L. B. Liang, A. A. Puretzky, K. Wang, J. J. Zheng, P. Yu, P. R. Pudasaini, A. W. Ghosh, Z. Liu, C. M. Rouleau, B. G. Sumpter, M. F. Chisholm, W. Zhou, P. D. Rack, D. B. Geohegan, K. Xiao, *J. Am. Chem. Soc.* **2017**, *139* 14090.

[3] D. Wu, J. W. Guo, J. Du, C. X. Xia, L. H. Zeng, Y. Z. Tian, Z. F. Shi, Y. T. Tian, X. J. Li, Y. H. Tsang, J. S. Jie, *ACS Nano* **2019**, *13* 9907.

[4] Y. D. Zhao, J. S. Qiao, P. Yu, Z. X. Hu, Z. Y. Lin, S. P. Lau, Z. Liu, W. Ji, Y. Chai, *Adv. Mater.* **2016**, *28* 2399.

[5] X. Y. Chia, A. Adriano, P. Lazar, Z. Sofer, J. Luxa, M. Pumera, *Adv. Funct. Mater.* **2016**, *26* 4306.

[6] G. Z. Wang, Z. Z. Wang, N. McEvoy, P. Fan, W. J. Blau, *Adv. Mater.* **2021**, *33* 2004070.

[7] Y. L. Wang, L. F. Li, W. Yao, S. R. Song, J. T. Sun, J. B. Pan, X. Ren, C. Li, E. Okunishi, Y. Q. Wang, E. Y. Wang, Y. Shao, Y. Y. Zhang, H. T. Yang, E. F. Schwier, H. Iwasawa, K. Shimada, M. Taniguchi, Z. H. Cheng, S. Y. Zhou, S. X. Du, S. J. Pennycook, S. T. Pantelides, H. J. Gao, *Nano Lett.* **2015**, *15* 4013.

[8] W. Yao, E. Y. Wang, H. Q. Huang, K. Deng, M. Z. Yan, K. N. Zhang, K. Miyamoto, T. Okuda, L. F. Li, Y. L. Wang, H. J. Gao, C. X. Liu, W. H. Duan, S. Y. Zhou, *Nat. Commun.* **2017**, *8* 14216.

[9] M. O'Brien, N. McEvoy, C. Motta, J. Y. Zheng, N. C. Berner, J. Kotakoski, K. Elibol, T. J. Pennycook, J. C. Meyer, C. Yim, M. Abid, T. Hallam, J. F. Donegan, S. Sanvito, G. S. Duesberg, *2D Mater.* **2016**, *3* 021004.

[10] Z. G. Wang, Q. Li, F. Besenbacher, M. D. Dong, *Adv. Mater.* **2016**, *28* 10224.

[11] C. Yim, K. Lee, N. McEvoy, M. O'Brien, S. Riazimehr, N. C. Berner, C. P. Cullen, J. Kotakoski, J. C. Meyer, M. C. Lemme, G. S. Duesberg, *ACS Nano* **2016**, *10* 9550.

[12] J. P. Shi, Y. H. Huan, M. Hong, R. Z. Xu, P. F. Yang, Z. P. Zhang, X. L. Zou, Y. F. Zhang, *ACS Nano* **2019**, *13* 8442.

[13] D. K. Hu, T. Q. Zhao, X. F. Ping, H. S. Zheng, L. Xing, X. Z. Liu, J. Y. Zheng, L. F. Sun, L. Gu, C. G. Tao, D. Wang, L. Y. Jiao, *Angew. Chem.-Int. Edit.* **2019**, *58* 6977.

[14] M. Z. Yan, E. Y. Wang, X. Zhou, G. Q. Zhang, H. Y. Zhang, K. N. Zhang, W. Yao, N. P. Lu, S. Z. Yang, S. L. Wu, T. Yoshikawa, K. Miyamoto, T. Okuda, Y. Wu, P. Yu, W. H. Duan, S. Y. Zhou, *2D Mater.* **2017**, *4* 045015.

[15] Y. D. Zhao, J. S. Qiao, Z. H. Yu, P. Yu, K. Xu, S. P. Lau, W. Zhou, Z. Liu, X. R. Wang, W. Ji, Y. Chai, *Adv. Mater.* **2017**, *29* 1604230.

[16] A. Ciarrocchi, A. Avsar, D. Ovchinnikov, A. Kis, *Nat. Commun.* **2018**, *9* 919.

[17] X. C. Yu, P. Yu, D. Wu, B. Singh, Q. S. Zeng, H. Lin, W. Zhou, J. H. Lin, K. Suenaga, Z. Liu, Q. J. Wang, *Nat. Commun.* **2018**, *9* 1545.

[18] Q. J. Liang, Q. X. Wang, Q. Zhang, J. X. Wei, S. X. D. Lim, R. Zhu, J. X. Hu, W. Wei, C. Lee, C. Sow, W. J. Zhang, A. T. S. Wee, *Adv. Mater.* **2019**, *31* 1807609.

[19] B. M. Szydlowska, O. Hartwig, B. Tywoniuk, T. Hartman, T. Stimpel-Lindner, Z. Sofer, N. McEvoy, G. S. Duesberg, C. Backes, *2D Mater.* **2020**, *7* 045027.

[20] X. Lin, J. C. Lu, Y. Shao, Y. Y. Zhang, X. Wu, J. B. Pan, L. Gao, S. Y. Zhu, K. Qian, Y. F. Zhang, D. L. Bao, L. F. Li, Y. Q. Wang, Z. L. Liu, J. T. Sun, T. Lei, C. Liu, J. O. Wang, K. Ibrahim, D. N. Leonard, W. Zhou, H. M. Guo, Y. L. Wang, S. X. Du, S. T. Pantelides, H. J. Gao, *Nat. Mater.* **2017**, *16* 717.

[21] S. D. Guo, *J. Mater. Chem. C* **2016**, *4* 9366.

[22] J. F. Xie, D. Zhang, X. Q. Yan, M. X. Ren, X. Zhao, F. Liu, R. X. Sun, X. K. Li, Z. Li, S. Q. Chen, Z. B. Liu, J. G. Tian, *2D Mater.* **2019**, *6* 035011.

[23] P. F. Li, L. Li, X. C. Zeng, *J. Mater. Chem. C* **2016**, *4* 3106.

[24] S. Sattar, U. Schwingenschlogl, *ACS Appl. Mater. Interfaces* **2017**, *9* 15809.

[25] Y. J. Yang, S. K. Jang, H. J. Choi, J. Xu, S. Lee, *Nanoscale* **2019**, *11* 21068.

[26] L. Li, K. C. Xiong, R. J. Marstell, A. Madjar, N. C. Strandwitz, J. C. M. Hwang, N. McEvoy, J. B. McManus, G. S. Duesberg, A. Goritz, M. Wietstruck, M. Kaynak, *IEEE Trans. Elec. Dev.* **2018**, *65* 4102.

[27] T. Y. Su, H. Medina, Y. Z. Chen, S. W. Wang, S. S. Lee, Y. C. Shih, C. W. Chen, H. C. Kuo, F. C. Chuang, Y. L. Chueh, *Small* **2018**, *14* 1800032.

[28] H. Xu, H. M. Zhang, Y. W. Liu, S. M. Zhang, Y. Y. Sun, Z. X. Guo, Y. C. Sheng, X. D. Wang, C. Luo, X. Wu, J. L. Wang, W. D. Hu, Z. H. Xu, Q. Q. Sun, P. Zhou, J. Shi, Z. Z. Sun, D. W. Zhang, W. Z. Bao, *Adv. Funct. Mater.* **2019**, *29* 1805614.

[29] F. Urban, F. Gity, P. K. Hurley, N. McEvoy, A. D. Bartolomeo, *Appl. Phys. Lett.* **2020**, *117* 193102.

[30] L. Ansari, S. Monaghan, N. McEvoy, C. O. Coileain, C. P. Cullen, J. Lin, R. Siris, T. Stimpel-Lindner, K. F. Burke, G. Mirabelli, R. Duffy, E. Caruso, R. E. Nagle, G. S. Duesberg, P. K. Hurley, F. Gity, *npj 2D Mater. Appl.* **2019**, *3* 33.

[31] M. A. U. Absor, I. Santoso, Harsojo, K. Abraha, F. Ishii, M. Saito, *Phys. Rev. B* **2017**, *96* 115128.

[32] A. Avsar, A. Ciarrocchi, M. Pizzochero, D. Unuchek, O. V. Yazyev, A. Kis, *Nat. Nanotechnol.* **2019**, *14* 674.

[33] J. Ge, T. C. Luo, Z. Z. Lin, J. P. Shi, Y. Z. Liu, P. Y. Wang, Y. F. Zhang, W. H. Duan, J. Wang, *Adv. Mater.* **2021**, *33* 2005465.

[34] C. Yim, N. McEvoy, S. Riazimehr, D. S. Schneider, F. Gity, S. Monaghan, P. K. Hurley, M. C. Lemme, G. S. Duesberg, *Nano Lett.* **2018**, *18* 1794.

[35] M. S. Long, F. K. Liu, F. Ding, Y. Wang, J. F. Ye, R. Z. Xie, H. Wang, M. J. Xu, F. Wang, Y. B. Tu, T. Han, F. Li, Z. Y. Zhang, L. W. Liu, *Appl. Phys. Lett.* **2020**, *117* 231104.

[36] Y. J. Yang, J. Li, S. Choi, S. Jeon, J. H. Cho, B. H. Lee, S. Lee, *Appl. Phys. Lett.* **2021**, *118* 013103.

[37] L. B. Luo, D. Wang, C. Xie, J. G. Hu, X. Y. Zhao, F. X. Liang, *Adv. Funct. Mater.* **2019**, *29* 1900849.

[38] Y. Wang, Z. J. Yu, Y. Y. Tong, B. L. Sun, Z. Y. Zhang, J. B. Xu, X. K. Sun, H. K. Tsang, *Appl. Phys. Lett.* **2020**, *116* 211101.

[39] Y. Wang, Z. J. Yu, Z. Y. Zhang, B. L. Sun, Y. Y. Tong, J. B. Xu, X. K. Sun, H. K. Tsang, *ACS Photo.* **2020**, *7* 2643.

[40] Y. W. Wang, Z. L. Deng, D. J. Hu, J. Yuan, Q. D. Ou, F. Qin, Y. N. Zhang, X. Ouyang, Y. Li, B. Peng, Y. Y. Cao, B. O. Guan, Y. P. Zhang, J. He, C. W. Qiu, Q. L. Bao, X. P. Li, *Nano Lett.* **2020**, *20* 7811.

[41] S. Wagner, C. Yim, N. McEvoy, S. Kataria, V. Yokaribas, A. Kuc, S. Pindl, C. P. Fritzen, T. Heine, G. S. Duesberg, M. C. Lemme, *Nano Lett.* **2018**, *18* 3738.

[42] C. C. Chung, H. Yeh, P. H. Wu, C. C. Lin, C. S. Li, T. T. Yeh, Y. Chou, C. Y. Wei, C. Y. Wen, Y. C. Chou, C. W. Luo, C. I. Wu, M. Y. Li, L. J. Li, W. H. Chang, C. W. Chen, *ACS Nano* **2021**, *15* 4627.

[43] W. Zhang, Z. Huang, W. Zhang, Y. Li, *Nano Res.* **2014**, *7* 1731.

[44] Q. Cui, R. A. Muniz, J. E. Sipe, H. Zhao, *Phys. Rev. B* **2017**, *95* 165406.

[45] H. Zhang, F. Ran, X. Shi, X. Fang, S. Wu, Y. Liu, X. Zheng, P. Yang, Y. Liu, L. Wang, X. Huang, H. Li, W. Huang, *Nanotechnology* **2017**, *28*, 16 164001.

[46] F. Ceballos, H. Zhao, *Adv. Funct. Mater.* **2017**, *27* 1604509.

[47] S. Q. Zhao, D. W. He, J. Q. He, X. W. Zhang, L. X. Yi, Y. S. Wang, H. Zhao, *Nanoscale* **2018**, *10* 9538.

[48] X. Chen, S. F. Zhang, L. Wang, Y. F. Huang, H. Y. Liu, J. W. Huang, N. N. Dong, W. M. Liu, I. M. Kislyakov, J. M. Nunzi, L. Zhang, J. Wang, *Photo. Res.* **2019**, *7* 1416.

[49] W. T. Qiu, W. Z. Liang, J. Guo, L. M. Fang, N. Li, Q. G. Feng, S. N. Luo, *J. Phys. D* **2021**, *54* 075102.

[50] G. Z. Wang, K. P. Wang, N. McEvoy, Z. Y. Bai, C. P. Cullen, C. N. Murphy, J. B. McManus, J. J. Mogan, C. M. Smith, G. S. Duesberg, I. Kaminer, J. Wang, W. J. Blau, *Small* **2019**, *15* 1902728.

[51] L. Wang, S. F. Zhang, N. McEvoy, Y. Y. Sun, J. W. Huang, Y. F. Xie, N. N. Dong, X. Y. Zhang, I. M. Kislyakov, J. M. Nunzi, L. Zhang, J. Wang, *Laser Photonics Rev.* **2019**, *13* 1900052.

[52] X. Zhao, F. Liu, D. Q. Liu, X. Q. Yan, C. F. Huo, W. W. Hui, J. F. Xie, Q. Ye, C. C. Guo, Y. Yao, Z. B. Liu, J. G. Tian, *Appl. Phys. Lett.* **2019**, *115* 263102.

[53] J. B. Fu, W. Q. Xu, X. Chen, S. F. Zhang, W. J. Zhang, P. Suo, X. Lin, J. Wang, Z. M. Jin, W. M. Liu, G. H. Ma, *J. Phys. Chem. C* **2020**, *124* 10719.

[54] J. D. Zhou, X. H. Kong, M. C. Sekhar, J. H. Lin, F. L. Goualher, R. Xu, X. W. Wang, Y. Chen, Y. Zhou, C. Zhu, W. Lu, F. C. Liu, B. J. Tang, Z. L. Guo, C. Zhu, Z. H. Cheng, T. Yu, K. Suenaga, D. Sun, W. Ji, Z. Liu, *ACS Nano* **2019**, *13* 10929.

[55] H. J. Shin, S. Bae, S. Sim, *Nanoscale* **2020**, *12* 22185.

[56] M. Sajjad, N. Singh, U. Schwingenschlogl, *Appl. Phys. Lett.* **2018**, *112* 043101.

[57] N. Kumar, Q. Cui, F. Ceballos, D. He, Y. Wang, H. Zhao, *Phys. Rev. B* **2014**, *89* 125427.

[58] D. Sun, Y. Rao, G. A. Reider, G. Chen, Y. You, L. Brezin, A. R. Harutyunyan, T. F. Heinz, *Nano Lett.* **2014**, *14* 5625.

[59] L. M. Smith, D. R. Wake, J. P. Wolfe, D. Levi, M. V. Klein, J. Klem, T. Henderson, H. Morkoç, *Phys. Rev. B* **1988**, *38* 5788.

[60] Y. Wan, Z. Guo, T. Zhu, S. Yan, J. Johnson, L. Huang, *Nat. Chem.* **2015**, *7* 785.

[61] H. Shi, R. Yan, S. Bertolazzi, J. Brivio, B. Gao, A. Kis, D. Jena, H. G. Xing, L. Huang, *ACS Nano* **2012**, *7* 1072.

[62] Q. Cui, F. Ceballos, N. Kumar, H. Zhao, *ACS Nano* **2014**, *8* 2970.

[63] R. Wang, B. A. Ruzicka, N. Kumar, M. Z. Bellus, H.-Y. Chiu, H. Zhao, *Phys. Rev. B* **2012**, *86* 045406.

[64] S. D. Stranks, G. E. Eperon, G. Grancini, C. Menelaou, M. J. P. Alcocer, T. Leijtens, L. M. Herz, A. Petrozza, H. J. Snaith, *Science* **2013**, *342* 341.

[65] G. C. Xing, N. Mathews, S. Y. Sun, S. S. Lim, Y. M. Lam, M. Gratzel, S. Mhaisalkar, T. C. Sum, *Science* **2013**, *342* 344.

[66] Z. Guo, Y. Wan, M. J. Yang, J. Snaider, K. Zhu, L. B. Huang, *Science* **2017**, *356* 59.

[67] D. Davydova, A. de la Cadena, D. Akimov, B. Dietzek, *Laser Photonics Rev.* **2016**, *10* 62.

[68] M. C. Fischer, J. W. Wilson, F. E. Robles, W. S. Warren, *Review of Scientific Instruments* **2016**, *87* 031101.

[69] N. S. Ginsberg, W. A. Tisdale, *Annu. Rev. Phys. Chem.* **2020**, *71* 1.

[70] D. A. Neamen, *Semiconductor Physics and Devices: Basic Principles*, McGraw-Hill, New York, **2011**.

[71] K. Saito, M. Okada, R. Kitaura, H. Kishida, T. Koyama, *Phys. Rev. B* **2021**, *103* L201401.

[72] H. Liu, C. Wang, Z. Zuo, D. Liu, J. Luo, *Adv. Mat.* **2020**, *32* 1906540.

[73] M. Kulig, J. Zipfel, P. Nagler, S. Blanter, C. Schuller, T. Korn, N. Paradiso, M. M. Glazov, A. Chernikov, *Phys. Rev. Lett.* **2018**, *120* 207401.

Table of Contents

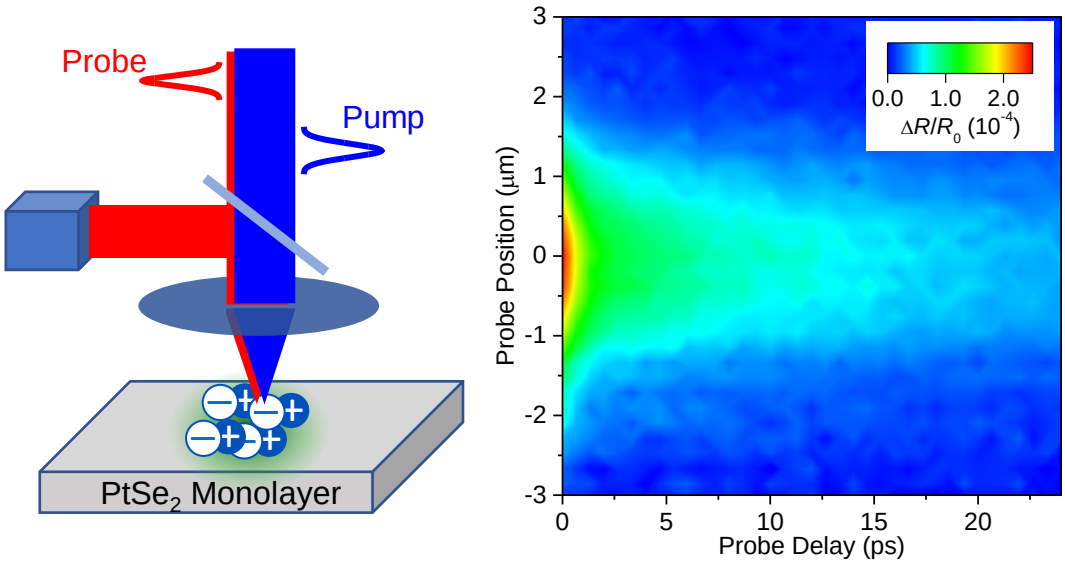

Fast exciton diffusion in monolayer $PtSe_2$ revealed by transient absorption microscopy